Carbon 120 (2017) 54–62

Contents lists available at ScienceDirect

Carbon

journal homepage: www.elsevier.com/locate/carbon

Carbon nanowalls: A new material for resistive switching memory devices

Paola Russo [a, b, *], Ming Xiao [a, b], Norman Y. Zhou [a, b, **]

[a] Waterloo Institute for Nanotechnology, University of Waterloo, 200 University Avenue West, Waterloo, Ontario N2L 3G1, Canada
[b] Centre for Advanced Materials Joining, Department of Mechanical and Mechatronics Engineering, University of Waterloo, 200 University Avenue West, Waterloo, Ontario N2L 3G1, Canada

ARTICLE INFO

Article history:
Received 17 February 2017
Received in revised form
13 April 2017
Accepted 4 May 2017
Available online 7 May 2017

ABSTRACT

In this work, we report for the first time the resistive switching behavior of a new type of device made of carbon nanowalls (CNWs) deposited on fluorine-doped tin oxide (FTO) substrate. This new device shows a forming-free bipolar resistive switching behavior, with a low operating voltage of 2 V and long retention time (5×10^{4} s). The CNWs are synthesized by electrophoretic deposition of a solution of polyynes obtained by arc discharge. We show that the environmentally-friendly and time-saving fabrication process we developed could overcome the current complex fabrication process of carbon-based memory devices which impede their large-scale development. The obtained results demonstrate the good reproducibility of the device's production process, and that the device's electrical performances can be engineered with a control of the fabrication parameters. The study presented suggests that CNWs are promising candidates for non-volatile memory devices and in carbon-based electronics.

1. Introduction

Currently, much attention is being paid to resistive switching random access memory (RRAM) devices as alternatives for the next generation of nonvolatile memories. The most common structure of a RRAM device consists of an insulator/semiconductor layer sandwiched between two metallic electrodes. The resistive switching (RS) behavior in this type of device is due to a resistance change between high resistance state (HRS) and low resistance state (LRS) when a voltage across the electrodes is applied [1–6]. Different types of RRAM have been fabricated based on the different chemical composition of the insulator/semiconductor layer and the different type of electrodes used. The materials that have been used for RRAM devices span from perovskites to transition metal oxides such as TiO_2, NiO, and ZnO to chalcogenides and recently organic dielectric materials have been used [7–20]. The underlying resistive switching mechanisms in RRAM devices depend on how the electron transport takes place in the sandwiched structure, which can be attributed to a large variety of physical and/or chemical phenomena. The mechanisms can be divided depending on whether the dominant contribution derives from a thermal, an ionic or an electronic effect [21,22]. It has been widely demonstrated that the presence of lattice defects in the switching layer plays a key role in the resistive switching performance of the RRAM devices [22]. The most common resistive switching mechanisms proposed in the current literature are: formation and rupture of conductive filaments induced by redox reactions, Schottky emission, space-charge-limited conduction (SCLC) controlled by the presence of defects in the materials, *i.e.* oxygen vacancies, that create charge-carrier traps, Pool-Frenkel emission, and trap-assisted tunneling where the RS originates from the electronic charge injection and/or charge displacements effects [1,3,4,21,23,24].

Carbon nanomaterials have been employed in a wide range of applications, and it has been reported that tetrahedral amorphous carbon films, graphene oxide and carbon nanotubes show resistive switching behavior, opening the possibility for their application for next-generation non-volatile memory devices [25–31]. Recently, Ageev and coworkers published an interesting study on the resistive switching behavior of vertically aligned carbon nanotubes (VA

* Corresponding author. Centre for Advanced Materials Joining, Department of Mechanical and Mechatronics Engineering, University of Waterloo, 200 University Avenue West, Waterloo, Ontario N2L 3G1, Canada.
** Corresponding author. Centre for Advanced Materials Joining, Department of Mechanical and Mechatronics Engineering, University of Waterloo, 200 University Avenue West, Waterloo, Ontario N2L 3G1, Canada.
E-mail addresses: p3russo@uwaterloo.ca (P. Russo), nzhou@uwaterloo.ca (N.Y. Zhou).

http://dx.doi.org/10.1016/j.carbon.2017.05.004
0008-6223/

CNT) under scanning tunneling microscopy (STM), induced by a distortion of the nanotubes upon the application of a voltage [29,32]. It was reported that the resistance ratio between the HRS and LRS was voltage dependent and reached 25 when 8 V was applied to the STM probe/VA CNT. However, no further studies on the main electrical performance parameters (i.e. endurance, retention time) have been carried out on VA CNT. In this connection, carbon nanowalls (CNWs) are two-dimensional nanomaterials made of graphene layers that instead of being rolled up as in VA CNT; they are vertically stacked onto a substrate leading to the formation of graphene "walls" [33]. These nanomaterials possess the characteristic properties of graphene together with unique characteristics induced by the presence of sharp edges and high surface area, which enable CNWs to be employed as field emitters, catalyst support, capacitors and in Li-ion battery fabrication [34–39]. Moreover, it is well known that graphene-like systems possess high electrical conductivity along the basal plane, and the CNWs, due to their perpendicular orientation structure, possess an enhanced electrical conductivity compared to graphene which promises to be employed for devices fabrication [40]. To the best of our knowledge no studies have been performed on whether CNWs can be employed for the application of memory devices. In this work, we report for the first time the resistive switching behavior of a new type of device made of CNWs on fluorine-doped tin oxide (FTO) substrates. This Al/CNWs/FTO device shows a forming-free bipolar RS behavior, with a low operating voltage of 2 V and long retention time (5×10^4s). The study presented here, shows that CNWs are promising candidates for the fabrication of non-volatile memory devices and their use in carbon-based electronics. In particular, the environmentally friendly and time saving fabrication process we developed could overcome the current complex fabrication process of carbon-based memory devices which impede their large-scale development [41]. The results presented here demonstrate the good reproducibility of the production process of the device, which electrical performances can be engineered with a systematic control of the fabrication parameters.

2. Experimental

The carbon nanowalls were obtained upon electrophoretic deposition of a solution of polyynes, which are linear carbon chains containing sp-carbon atoms [42]. The polyynes acted as building blocks for the fabrication of the carbon nanowalls and a similar fabrication method has been already published employing polyynes obtained by laser ablation of a graphite target and then deposited by electrophoresis [43]. The details about the synthesis of polyynes and their EPD for the synthesis of the CNWs are given below.

2.1. Synthesis of the polyynes

In this work the polyynes were obtained by arc discharge in water between two graphite electrodes having a diameter of 10 mm and length 70 mm [42,44,45]. The arc discharge between the electrodes was maintained for 10 min at a voltage of 30 V. In Fig. S1a picture of the arc discharge setup is displayed while in Fig. S2 is shown the UV/VIS spectrum of the obtained polyynes. In particular polyynes containing 6, 8 and 10 carbon atoms per chain were produced [46].

2.2. Synthesis and deposition of the carbon nanowalls

The polyynes solution was transferred in a glass beaker and two pieces of FTO/glass substrate were used as electrodes and submerged in the polyynes solution. The distance between the two electrodes during the electrophoretic deposition was kept at 5 mm. The FTO substrates, with a resistance of ~10 Ω sq^{-1}, before the polyynes deposition and fabrication of the CNWs, were cleaned in acetone, ethanol and isopropyl alcohol respectively and dried under nitrogen gas flow. The CNWs deposition occurred at the cathode upon application of a voltage of 30 V at the electrodes for 1 h. The CNWs/FTO substrate was then annealed at 150 °C for 1 h in Argon gas, in order to remove the trapped water. In total three types of heat treatments of the CNWs have been carried out: heat treatment at 150 °C in argon, in air and in argon followed by heat treatment in air.

2.3. Fabrication of the memory device

Al top electrodes with 100 nm thickness and 1 mm diameter were deposited by an e-beam evaporation process on the CNWs surface.

2.4. Characterizations

Scanning Electron Microscopy (SEM) analyses have been performed using a ZEISS LEO 1550 FE-SEM at an accelerating voltage of 5 kV. The X-ray photoelectron spectroscopy (XPS) analysis was carried out using a multi-technique ultra-high vacuum imaging XPS microprobe spectrometer (Thermo VG Scientific ESCALab 250) with a monochromatic Al-Ka 1486.6 eV X-ray source. The spectrometer was calibrated by Au 4f7/2 (binding energy of 84.0 eV) with respect to the Fermi level. The chamber vacuum level was maintained below 2×10^{-10} Torr. The carbon nanowalls were analyzed using a Renishaw In Via micro-Raman spectrometer, employing an excitation laser with a wavelength of 633 nm, and the spectra were acquired with a 50× objective at a laser power of 0.1 mW. HRTEM observation was conducted using a JEOL 2010F at the Canadian Centre for Electron Microscopy (Hamilton, Ontario, Canada). TEM samples were prepared by scratching the samples onto lacey carbon grids. Electrical measurements have been performed with a Keithley 2602A source meter at ambient conditions.

3. Results and discussion

The new CNWs-memory devices were fabricated in three steps using arc discharge and electrophoretic deposition (EPD) for the synthesis and deposition of CNWs on FTO substrate, respectively. Arc discharge in water of two graphite electrodes was employed for the production of a solution of polyynes, which are linear carbon chains of sp-carbon atoms [42,44,45]. These nanomaterials were then used as building blocks for the synthesis of the CNWs; indeed polyynes have a strong tendency to interchain crosslinking. The EPD was used for the synthesis/deposition of CNWs on FTO substrate, since it has been demonstrated as an excellent method to deposit carbon nanomaterials for forming free RRAM devices [47]. FTO substrates were used as electrodes and immersed in the polyynes solution. Upon application of the electric field, the polyynes are transported at the cathode and undergo interchain crosslinking reactions leading to the formation of hexagonal-graphene like sp^2 carbon structures perpendicular to the electrode's surface, *i.e.* the CNWs [48,49]. After heat treatment in Argon at 150 °C for 1 h, the final step of the fabrication process was the deposition of Al top electrodes on the CNWs/FTO substrate by e-beam evaporation. The production method we developed is more user-friendly, cost-effective and eco-friendly compared to the current fabrication methods employed for the synthesis of carbon-based electronic devices, since no high temperatures or high pressures and poisonous chemicals are needed [41]. Fig. 1a displays a schematic of the structure of the Al/CNWs/FTO devices fabricated, while in

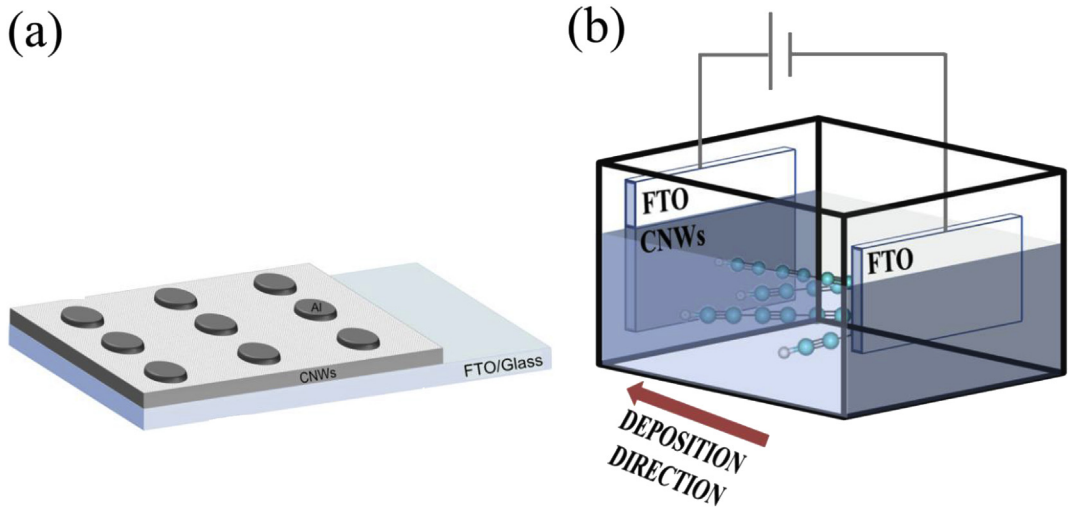

Fig. 1. (a) Schematic design of the structure of the Al/CNWs/FTO device, (b) schematic of the apparatus for the EPD of polyynes in order to obtain the CNWs. (A colour version of this figure can be viewed online.)

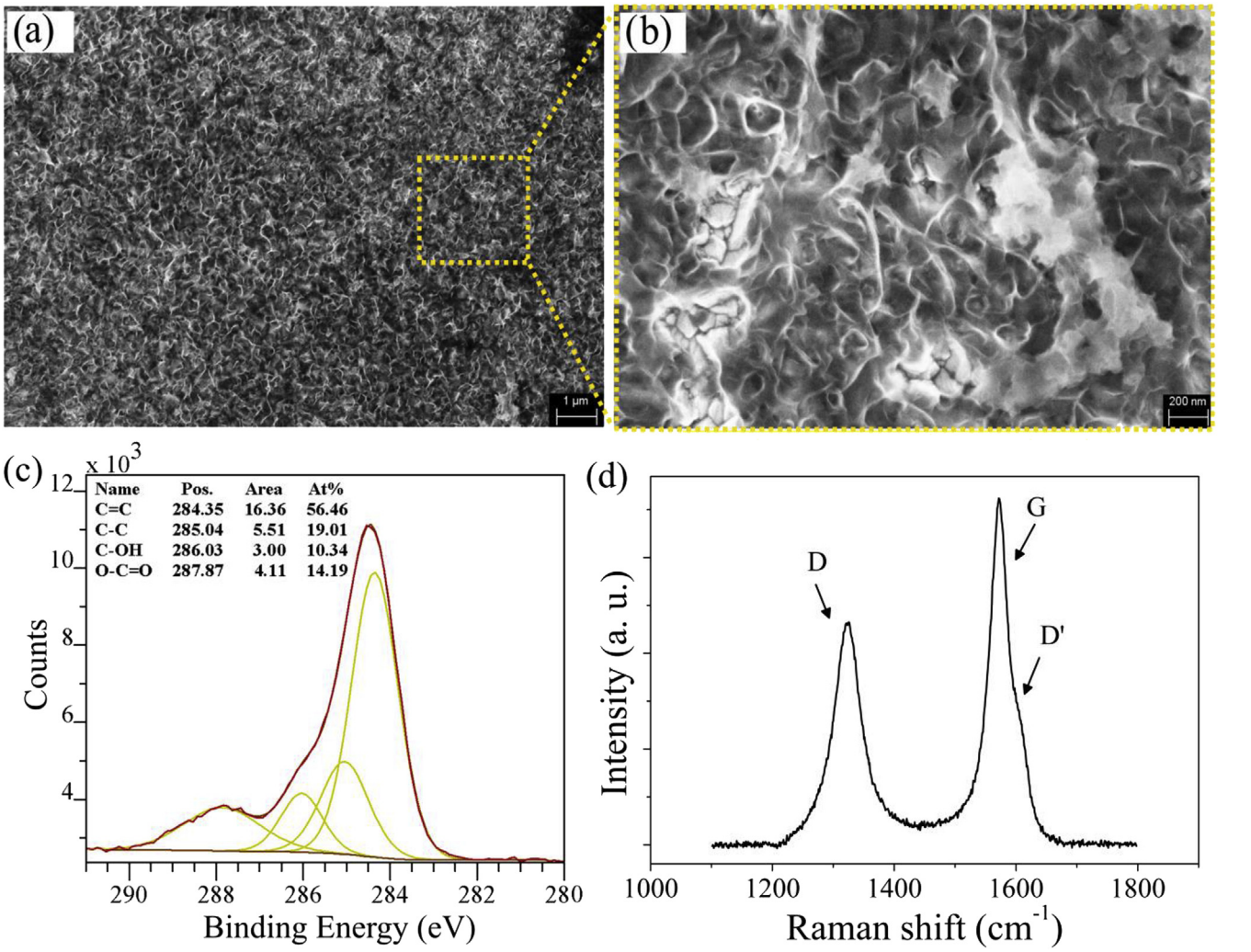

Fig. 2. a) SEM image of the surface morphology of the CNWs prepared by EPD of polyynes. b) Magnification of the CNWs surface morphology. c) C1s XPS and (d) Raman spectrum of the CNWs. (A colour version of this figure can be viewed online.)

Fig. 1b a schematic of the EPD process is displayed. The top-view SEM image of the CNWs obtained after the EPD of polyynes on FTO substrate is shown in Fig. 2a which confirmed that the CNWs are uniformly distributed over the substrate area. In Fig. 2b is displayed the magnified SEM image of the CNWs. The SEM images show the typical morphology of the carbon nanowalls, where the branched 2-dimensional carbon sheets are clearly shown.

Fig. 2c presents the C1s XPS spectrum of the electrophoretic fabricated CNWs. The C1s peak was fitted using a Gaussian-Lorentzian curve to four components in which the peak located at 284.35 eV indicates the presence of sp^2 carbon atoms (C=C), the peak at 285.04 eV is attributed to sp^3 carbon atoms (C-C), while the peaks at 286.03 eV and 287.87 eV can be ascribed to (C-OH) and (-O-C=O) groups respectively [43,50]. As shown in the inset in Fig. 2c, the percentage of sp^2 carbon atoms is 56.46%, while the ratio relative to sp^3 carbon atoms is 19.01%, due to the presence of defect sites or edges [51]. The presence of 10.34% of hydroxyl groups and 14.19% of (-O-C=O) groups also suggest that a mild oxidation of the carbon nanowalls occurs during the fabrication process. The formation of defects and presence of oxygen-containing groups upon fabrication of CNWs by EPD is crucial for the resistive switching behavior of the device [21,22].

The CNWs were analyzed by Raman spectroscopy with an excitation wavelength of 633 nm and the relative spectrum is displayed in Fig. 2d. It is possible to notice, that the Raman spectrum obtained is the one characteristic of CNWs, as reported by Kurita and Wang [52,53]. In particular, it can be observed the characteristic D band originated by the presence of defects and the G band which arises from the in-plane vibration of sp^2 carbon atoms. As reported by Kurita [52], the narrow G band (~37 cm^{-1}) is due to the presence of nanowalls made of small crystallites with high degree of graphitization. In addition to these bands, a weak band is also observed corresponding to D′ band originated by the presence of disorder. The length of the carbon nanowalls can be correlated to the I_D/I_G ratio, since it increases with decreasing the CNWs [52]. The I_D/I_G ratio of the CNWs is 0.95 (see Fig. S3) and based on the literature the length of our CNWs should be around 1.8 μm [52]. It is also reported that a decrease of the I_D/I_G ratio occurs upon addition of O_2 [53,54]. From Fig. 2b it is possible to notice that the CNWs are smaller in length than 1.8 μm, therefore the low I_D/I_G ratio could be

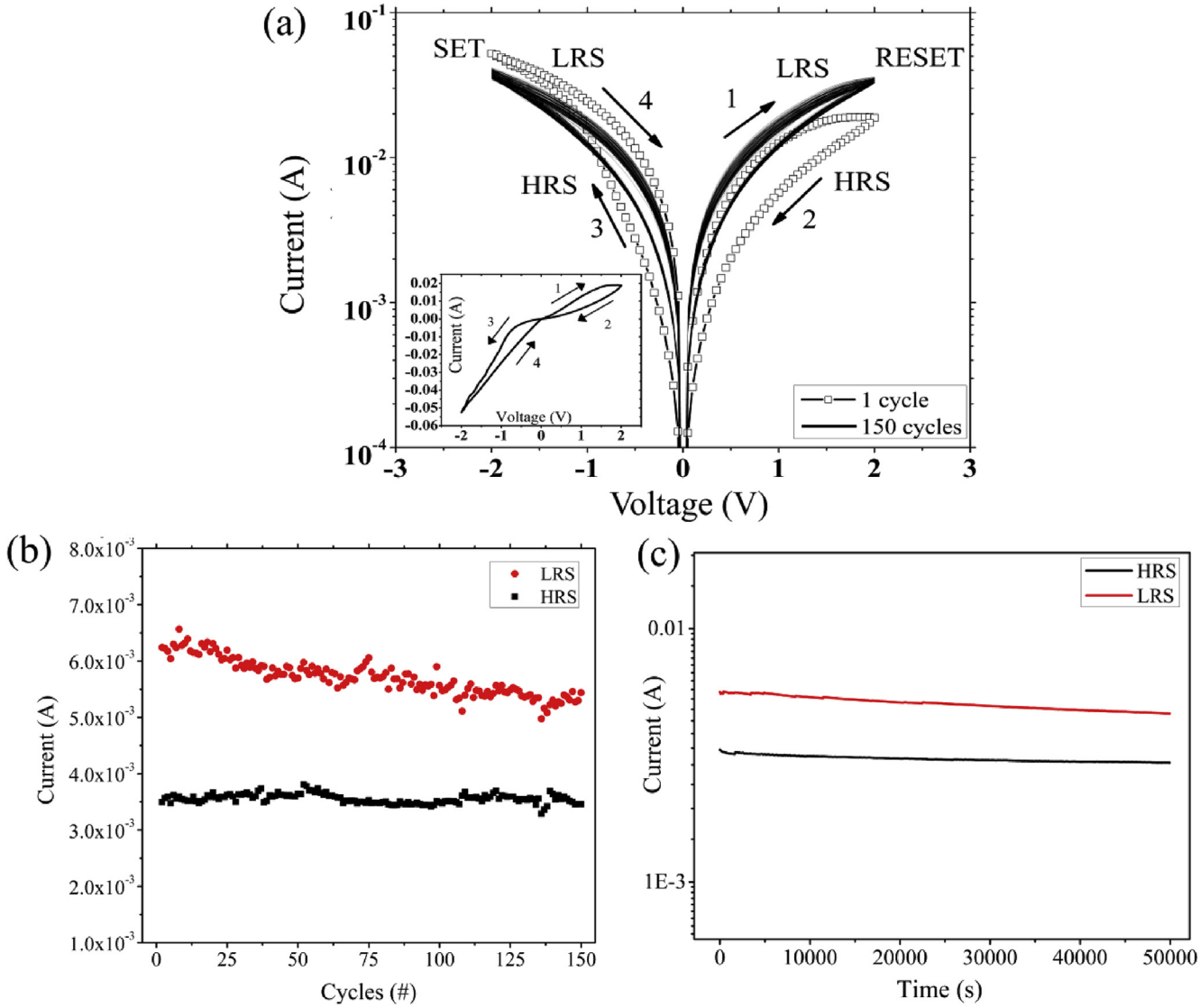

Fig. 3. a) I-V curve of Al/CNWs/FTO device for first and 150 cycles of voltage sweeping. Arrows and numbers indicate the direction and sequence for the I–V scan. b) Endurance results of the device for over 150 cycles at 0.4 V. c) Retention result over 5×10^4 s at a read voltage of 0.4 V. (A colour version of this figure can be viewed online.)

attributed to the presence of oxygen groups which induce a mild oxidation of the CNWs. From the TEM results displayed in Fig. S4 in the Supplementary data it is possible to notice that, the CNWs are made of 8–10 graphene layers with a d-spacing of 0.34 nm, which is the interlayer distance in graphite. These results together with the SEM and Raman analysis, confirm the synthesis of carbon nanowalls.

The electrical performance of the fabricated Al/CNWs/FTO devices was investigated by applying the sweep voltages of 0 V → 2 V → 0 V → −2 V → 0 V. Fig. 3a demonstrates the typical bipolar resistive switching behavior of the new developed device obtained under direct sweeping operations for 1 and 150 cycles. It was found that the Al/CNWs/FTO device was initially in the LRS and the device maintained this state during the voltage sweeping from 0 to 2 V. The reason might be due to the dominance of sp^2 carbon atoms over the sp^3, providing high conducting channels in the CNWs [55], as confirmed by XPS study in Fig. 2c. Moreover, as aforementioned, the vertical orientation of the CNWs parallel to the electrons flow causes a higher conductivity [40], leading to the initial LRS in our I-V current response. The device switches to the HRS during the voltage sweeping from 2 V to 0 V, which means that the RESET process occurs. The HRS remained after the negative voltage was applied until the negative voltage is high enough to transition the device from HRS to LRS. It should be noted that the resistive switching performance for our devices does not require the commonly used electroforming step [55], desirable for the ReRAM devices due to the simplifying electrical operation.

We have observed that the I-V curve obtained after 150 cycles is different from the one obtained after only one cycle and we hypothesize this could be attributed to a rearrangement of the oxygen atoms in the CNWs structure induced by the first voltage sweep. The reset and set currents slightly changed after the first cycle and stabilized with increasing the number of cycles. After 150 cycles it was still possible to distinguish the LRS and HRS, suggesting that this new type of device could be employed as RRAM in future memory devices. The results of the cycling performance are shown in Fig. 3b at the read voltage of 0.4 V. Over 150 cycles we found that the difference between the LRS and HRS firstly decreased but the difference remained constant with increase in the number of cycles probably as a consequence of the stabilization of CNWs structure, suggesting a promising durability of the new device. Fig. 3c shows the retention results measured at room temperature. Over the time period of 5×10^4 s, the currents for HRS and LRS, respectively measured at 0.4 V were stable, confirming the non-volatile nature of the device.

It is important to explore the origin of the RS effect in this new type of CNWs-based devices. Based on the type of the dielectric layer sandwiched between the electrodes, the RS behavior has been explained with different types of mechanisms [3,6,23]. In order to study the RS mechanism in our device, the I-V curves have been fitted to the different mechanisms and among them we found that the trap-controlled SCLC mechanism, which is controlled by the presence of defects, best fit our device. The structural defects are related to the following mechanism for the formation of the CNWs upon EPD of polyynes. As aforementioned, polyynes are characterized by an extremely high reactivity with oxygen and a strong tendency to interchain crosslinking. Therefore, when polyynes are transported at the surface of electrode upon application of the electric field, interchain crosslinking reactions occur leading to the synthesis/deposition of CNWs [48,49]. The deposition process and the crosslinking reactions might lead to the formation of defective carbon structures (pentagon rings) with missing carbon atoms, which results in the formation of defect sites in the CNWs. The presence of defect sites and oxygen is confirmed by the observation of the peak at 285.04 eV attributed to sp^3 carbon atoms (related to the presence of defect sites) and the peaks at 286.03 eV and 287.87 eV (related to oxygen containing carbon groups), as seen in the XPS spectrum in Fig. 2c. Therefore, we hypothesize that due to the presence of structural defects and oxygen in the CNWs, the RS effect observed in our new device can be explained with the trap-controlled SCLC mechanism. In order to verify this hypothesis, we replotted the I-V curves of the device heat treated in argon in double-logarithmic scale as shown in Fig. 4.

The I-V curve characteristic of trap-controlled SCLC can be easily recognized since the HRS consists of three portions: (i) Ohmic region ($I \propto V$) observed at low field; (ii) the Child's Law region ($I \propto V^2$); (iii) steep current increase observed at high field [23]. It can be seen that the I-V curves are in agreement with the trap-controlled SCLC mechanism. In particular, under positive voltage the LRS follows the Ohm's law conduction mechanism with a slope ~1, i.e., current varies linearly with applied voltage, while the HRS consists of two regions. At low voltage the current conduction follows the Ohm's law with a slope of ~1 and at higher voltage the Child's law conduction mechanism is dominant, suggesting that the switching

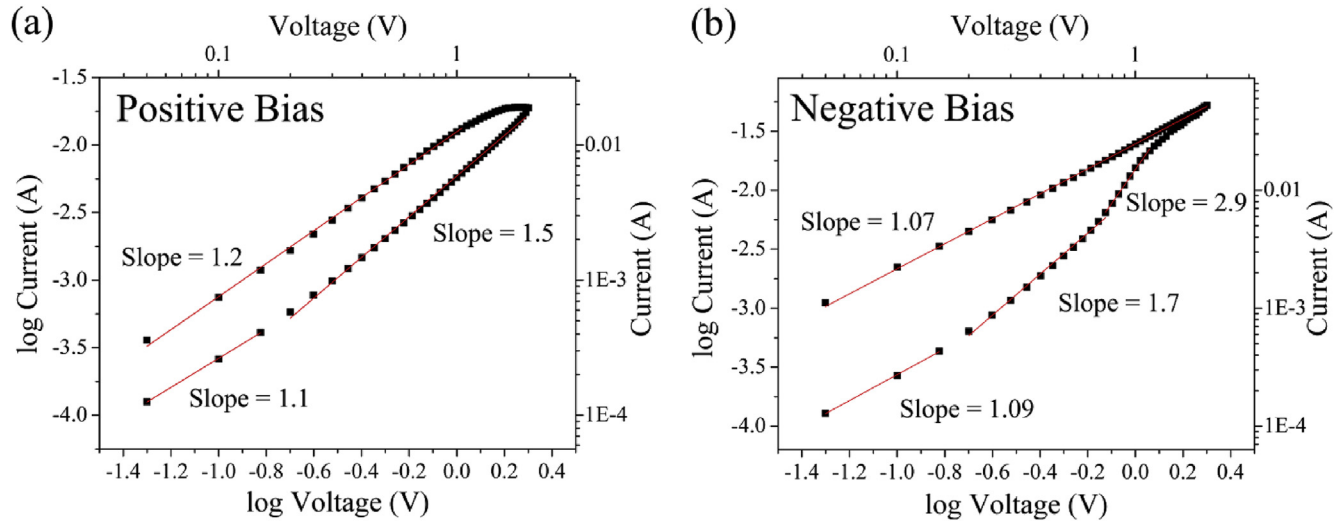

Fig. 4. SCLC I-V characteristics of the Al/CNWs/FTO device plotted in double-logarithmic scale for the a) positive and b) negative bias. (A colour version of this figure can be viewed online.)

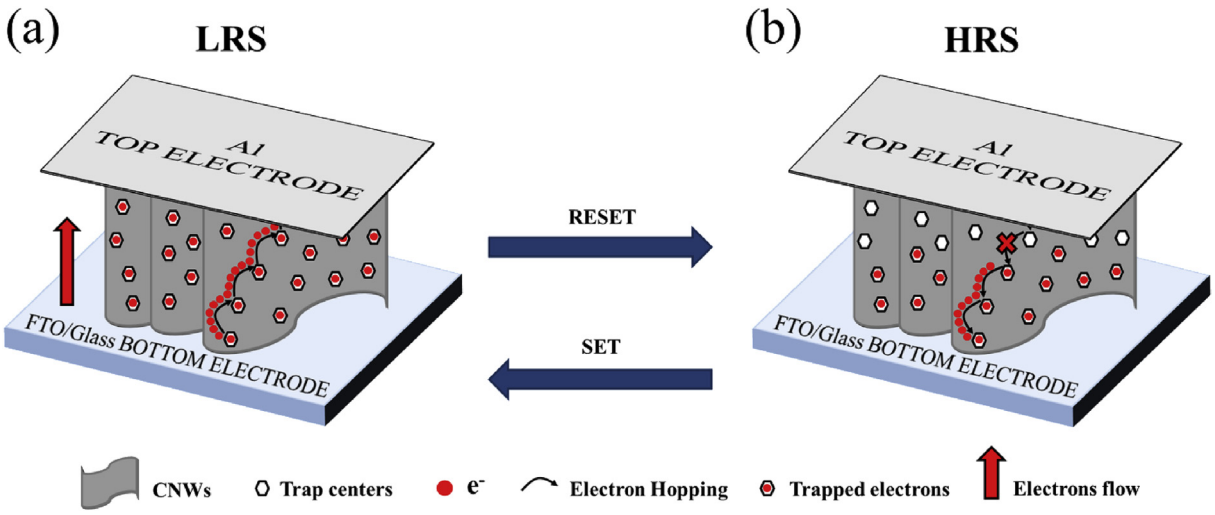

Fig. 5. Schematic showing the RS mechanism of the Al/CNWs/FTO device. (a) The LRS after applying a positive bias. The electrons flow along the filled oxygen vacancies from the bottom FTO electrode to the top Al electrode without the requirement of a forming step. (b) Transitioning from LRS to HRS caused by a de-trapping process of electrons from the oxygen vacancies upon application of a negative bias. (A colour version of this figure can be viewed online.)

mechanism is controlled by the trap-controlled SCLC. The slope value is lower than the one reported for the Child's law mechanism, however lower slope values have been recorded in case of conjugated polymers and CNWs are made of conjugated carbon atoms [56]. Under negative voltage, the LRS was found to follow the Ohm's law, while the HRS showed three regions: at low voltage the conduction mechanism followed the Ohm's law with a slope of 1. The intermediate region represents the transition between Ohm's and Child's law conduction mechanisms [57]. The third region with slope 2.9 was seen to correspond to the Child's law region [57].

From the above results we determined that the initial state of the device is LRS due to: (i) existence of defects sites, i.e. oxygen vacancies, which act as trap centers for the electrons and (ii) the perpendicular orientation of the CNWs on the FTO substrate which enhances the electrical conductivity. Therefore, upon the application of a positive bias the electrons could flow along the filled oxygen vacancies from the bottom FTO electrode to the top Al electrode without the requirement of a forming step. Upon the application of negative bias, a de-trapping process of electrons from the oxygen vacancies occurs, which causes the device to transition from LRS to HRS. A schematic of the RS mechanism is shown in Fig. 5.

These preliminary results indicated that the morphology of CNWs plays a key role in the electrical performance of the device. In particular, we showed that the presence of defects sites, i.e. oxygen vacancies, is vital for the RS behavior of the CNWs based devices. Therefore, it was of interest to try to engineer the concentrations of defects in the CNWs structure and study how the RS performance is affected. Heat treatment of carbon nanomaterials is a way that can be employed for the modulation of oxygen containing groups [58], which might affect the RS behavior. Therefore, after 1 h of deposition of CNWs by EPD on FTO substrate, the substrate was heat treated at 150 °C in air at ambient pressure. The electrical performance was then investigated and compared to the sample heat

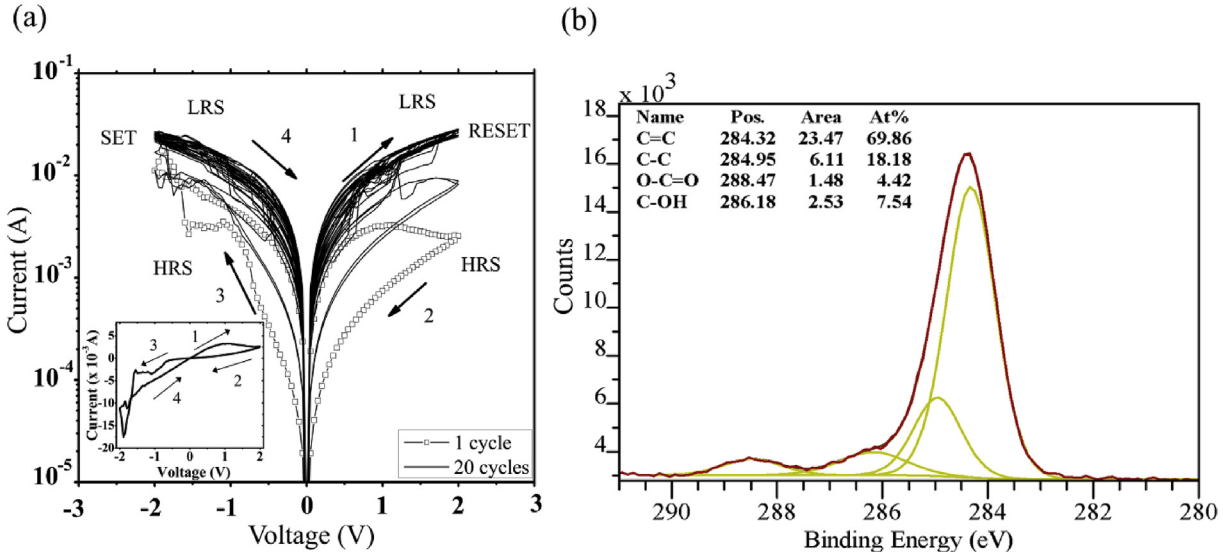

Fig. 6. a) Resistive switching characteristic after 1 and 20 cycles of the Al/CNWs/FTO device heat treated in air. b) C 1s XPS spectrum of the CNWs heat treated in air. (A colour version of this figure can be viewed online.)

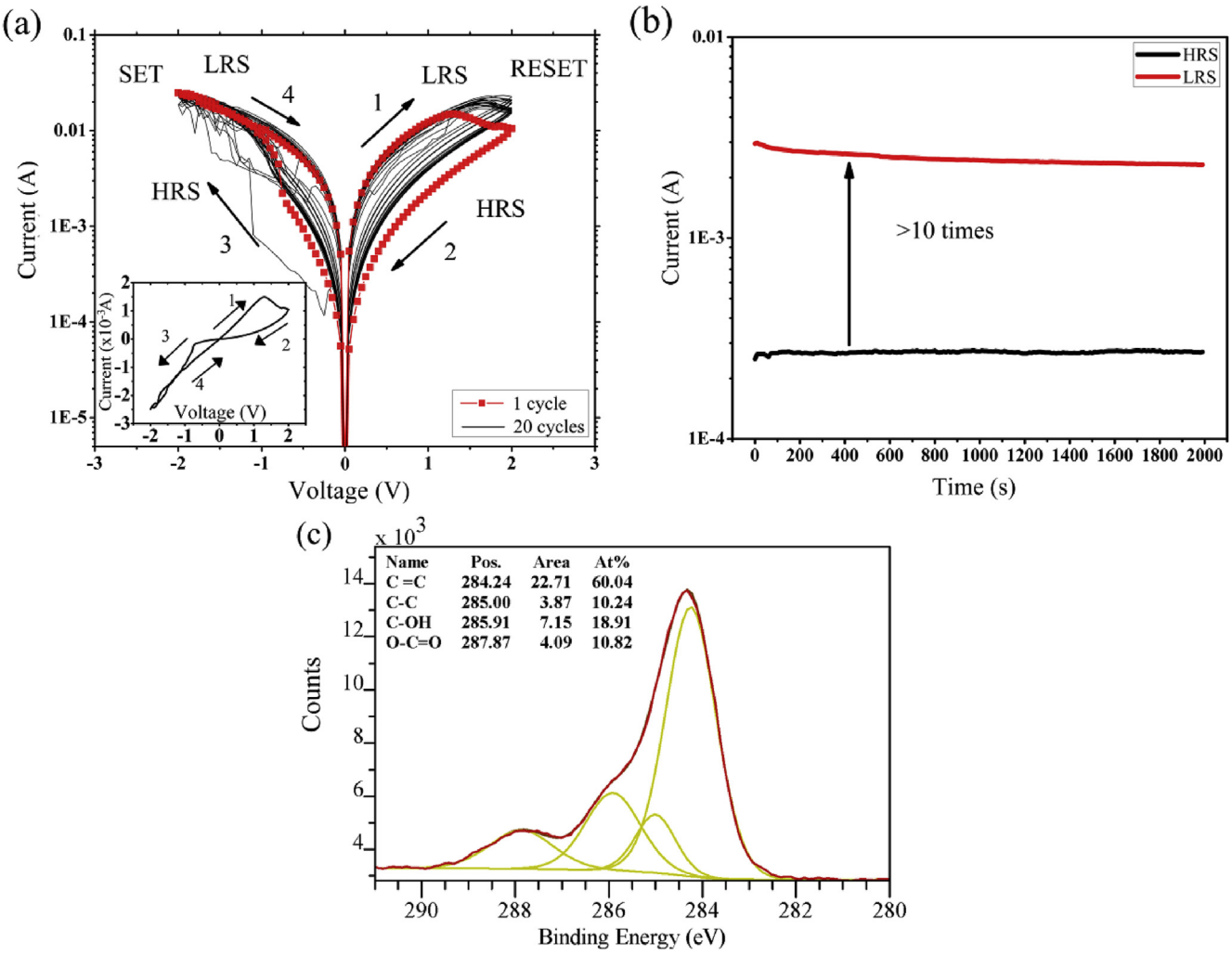

Fig. 7. a) I-V characteristics after 1 and 20 cycles at a sweeping voltage of 2 V. b) retention of the device at 0.2 V. c) XPS spectrum of C 1s. (A colour version of this figure can be viewed online.)

treated in argon at 150 °C. In Fig. 6 are shown the I-V characteristics of the device heat treated in air under the voltage sweep of 2 V.

Fig. 6a shows that the RS behavior is similar to the device heat treated in argon, with the device initially in the LRS state. Noteworthy, the LRS/HRS ratio after one voltage sweep at 2 V was higher for the sample heat treated in air than the one heat treated in argon (LRS/HRS of 7 and 3 respectively at the read voltage of 0.4 V); however, the device did not show a good endurability. In particular, after few cycles the device became unstable and the LRS and HRS became undistinguishable, as displayed in Fig. 6a. Clearly, this demonstrates that the heat treatment conditions after the deposition process play a key role in the stability of the device. The reason for the instability of the device might be the presence of a higher percentage of sp^2 carbon atoms and a lower percentage of oxygen containing carbon groups after the treatment in air atmosphere. In Fig. 6b the XPS spectrum of C1s is displayed together with the atomic percentages (inset) of carbon atoms and carbon groups detected in the sample. It was found that compared to the XPS spectrum of the sample heat treated in argon (Fig. 2c), in the sample treated in air the percentage of sp^2 carbon atoms increased by ~ 24%, while the percentage of hydroxyl groups and carboxyl groups were 7.54% and 4.42%, respectively. This result suggests, supported by the current literature, that the heat treatment in air at 150 °C induced a reduction of the CNWs [59], leading to a restoration of the sp^2 hybridization and a decrease in the oxygen containing groups. The heat treatment in air leads to more conductive and less defective CNWs in term of oxygen containing groups compared to the CNWs heat treated in argon and this could be the reason for the instability of the device. In particular, as aforementioned, the presence of defects, i.e. oxygen vacancies, plays a key role in the RS behavior of our device and the fact that the heat treatment in air led to CNWs with less content of oxygen and higher content of sp^2 carbon atoms might affect the RS behavior. This result leads us to the hypothesis that the fabrication of CNWs with a smaller percentage of sp^2 carbon atoms and higher percentage of oxygen containing carbon groups could lead to more stable devices [55]. In order to confirm our hypothesis a preliminary experiment was carried out with heat treatment of the CNWs first in argon, in order to remove the trapped water molecules, followed by heat treatment in air at 150 °C. In Fig. 7a, the I-V characteristics after sweeping a voltage of 2 V for 1 cycle and after 20 cycles are displayed. We noticed that after one cycle the LRS/HRS ratio reached a value of 9, however the device was not very stable and after few cycles the LRS and HRS collapsed. The retention experiment carried out at a voltage of 0.2 V showed that the device was able to maintain the LRS and HRS up to 2000 s with a ratio of ~10. Compared to the device heat treated only in argon and only in air, we found that the new type of heat treatment increased the

LRS/HRS ratio but it did not result in an increase of stability in terms of endurability of the device. The XPS analysis (Fig. 7c) showed that the heat treatment in argon and in air increased the sp^2 percentage compared to the CNWs heat treated only in argon, as well as the percentage of oxygen containing groups. From these preliminary results we can assess that the control of the content of sp^2 carbon atoms and oxygen groups is crucial for the stability of the CNWs device. In particular, on one side a higher content of sp^2 carbon atoms leads to devices with a higher LRS/HRS ratio, which promise to be employed for the fabrication of high-density memory devices [6]. On the other side it seems that the increase of sp^2 carbon atoms together with the decrease of oxygen containing groups affect the RS behavior due to a decrease in the concentration of charge-carrier traps, which are vital for the RS behavior. Therefore, our hypothesis is that highly oxidized carbon nanowalls, with a lower percentage of sp^2 carbon atoms might be employed for the fabrication of more stable memory devices.

4. Conclusions

In summary, for the first time we demonstrated the resistive switching behavior of a new type of device made of carbon nanowalls on FTO substrates via EPD. The electrical measurements indicate that the Al/CNWs/FTO device shows a forming-free bipolar RS behavior, with a low operating voltage of 2 V and long retention time (5×10^4s), confirming the nonvolatile nature of the device. Moreover, the fabrication method of CNWs by EPD is worthy of attention. Here we demonstrated that arc discharge in water followed by EPD can be employed for the synthesis of CNWs under environmentally friendly and timesaving conditions. It is clear that the device is still in its early stage of development, and we found out that heat treatment of the deposited layer of CNWs plays a key role in the stability of the device. In particular, based on the experiments we found a dependence of the stability of the device on the oxygen content in CNWs. Therefore, we hypothesize that higher oxygen content might lead to much more stable electrical performance and with proper control of this parameter, this new type of materials can be employed for non-volatile memory devices and other carbon-based electronics.

Acknowledgments

The work is supported by the Natural Science and Engineering Council of Canada (NSERC, Canada).

Appendix A. Supplementary data

Supplementary data related to this article can be found at http://dx.doi.org/10.1016/j.carbon.2017.05.004.

References

[1] P. Mazumder, S.M. Kang, R. Waser, Memristors: devices, models, and applications [scanning the issue], Proc. IEEE 100 (2012) 1911–1919, http://dx.doi.org/10.1109/JPROC.2012.2190812.
[2] L.O. Chua, Memristor—the missing circuit element, IEEE Trans. Circuit Theory 18 (1971) 507–519, http://dx.doi.org/10.1109/TCT.1971.1083337.
[3] I. Valov, R. Waser, J.R. Jameson, M.N. Kozicki, Electrochemical metallization memories–fundamentals, applications, prospects, Nanotechnology 22 (2011) 254003, http://dx.doi.org/10.1088/0957-4484/22/28/289502.
[4] F. Pan, C. Chen, Z. Wang, Y. Yang, J. Yang, F. Zeng, Nonvolatile resistive switching memories-characteristics, mechanisms and challenges, Prog. Nat. Sci. Mater. Int. 20 (2010) 1–15, http://dx.doi.org/10.1016/S1002-0071(12)60001-X.
[5] B.P. Mazumder, F. Ieee, Memristors: Devices, Models, and Applications, vol. 100, 2012, pp. 1911–1919.
[6] Y. Li, S. Long, Q. Liu, H. Lü, S. Liu, M. Liu, An overview of resistive random access memory devices, Chin. Sci. Bull. 56 (2011) 3072–3078, http://dx.doi.org/10.1007/s11434-011-4671-0.
[7] E. Gale, TiO_2-based memristors and ReRAM: materials, mechanisms and models (a review), Semicond. Sci. Technol. 29 (2014) 104004, http://dx.doi.org/10.1088/0268-1242/29/10/104004.
[8] C.-H.H. Huang, J.-S.S. Huang, S.-M.M. Lin, W.-Y.Y. Chang, J.-H.H. He, Y.-L.L. Chueh, ZnO_{1-x} nanorod arrays/ZnO thin film bilayer structure: from homojunction diode and high-performance memristor to complementary 1D1R application, ACS Nano 6 (2012) 8407–8414, http://dx.doi.org/10.1021/nn303233r.
[9] D.S. Jeong, R. Thomas, R.S. Katiyar, J.F. Scott, H. Kohlstedt, A. Petraru, C.S. Hwang, Emerging memories: resistive switching mechanisms and current status, Rep. Prog. Phys. 75 (2012) 76502, http://dx.doi.org/10.1088/0034-4885/75/7/076502.
[10] L. Lin, L. Liu, K. Musselman, G. Zou, W.W. Duley, Y.N. Zhou, Plasmonic-radiation-enhanced metal oxide nanowire heterojunctions for controllable multi-level memory, Adv. Funct. Mater. (2016) 5979–5986, http://dx.doi.org/10.1002/adfm.201601143.
[11] Z.J. Liu, J.Y. Gan, T.R. Yew, ZnO-based one diode-one resistor device structure for crossbar memory applications, Appl. Phys. Lett. 100 (2012) 153503, http://dx.doi.org/10.1063/1.3701722.
[12] R. Mundle, C. Carvajal, A.K. Pradhan, ZnO/Al:ZnO transparent resistive switching devices grown by atomic layer deposition for memristor applications, Langmuir 32 (2016) 4983–4995, http://dx.doi.org/10.1021/acs.langmuir.6b01014.
[13] S. Nau, C. Wolf, K. Popovic, A. Blümel, F. Santoni, A. Gagliardi, A. di Carlo, S. Sax, E.J.W. List-Kratochvil, Inkjet-printed resistive switching memory based on organic dielectric materials: from single elements to array technology, Adv. Electron. Mater. 1 (2015) 1400003, http://dx.doi.org/10.1002/aelm.201400003.
[14] K. Oka, T. Yanagida, K. Nagashima, M. Kanai, T. Kawai, J.S. Kim, B.H. Park, Spatial nonuniformity in resistive-switching memory effects of nio, J. Am. Chem. Soc. 133 (2011) 12482–12485, http://dx.doi.org/10.1021/ja206063m.
[15] K. Oka, T. Yanagida, K. Nagashima, T. Kawai, J.S. Kim, B.H. Park, Resistive-switching memory effects of NiO nanowire/metal junctions, J. Am. Chem. Soc. 132 (2010) 6634–6635, http://dx.doi.org/10.1021/ja101742f.
[16] S. Porro, A. Jasmin, K. Bejtka, D. Conti, D. Perrone, S. Guastella, C.F. Pirri, A. Chiolerio, C. Ricciardi, Low-temperature atomic layer deposition of TiO_2 thin layers for the processing of memristive devices, J. Vac. Sci. Technol. A Vac. Surf. Film 34 (2016) 01A147, http://dx.doi.org/10.1116/1.4938465.
[17] J.P. Strachan, J.J. Yang, L.A. Montoro, C.A. Ospina, A.J. Ramirez, A.L.D. Kilcoyne, G. Medeiros-Ribeiro, R.S. Williams, Characterization of electroforming-free titanium dioxide memristors, Beilstein J. Nanotechnol. 4 (2013) 467–473, http://dx.doi.org/10.3762/bjnano.4.55.
[18] H. Wang, B. Zhu, X. Ma, Y. Hao, X. Chen, Physically transient resistive switching memory based on silk protein, Small 12 (2016) 2715–2719, http://dx.doi.org/10.1002/smll.201502906.
[19] M. Xiao, K.P. Musselman, W.W. Duley, N.Y. Zhou, Resistive switching memory of TiO_2 nanowire networks grown on Ti foil by a single hydrothermal method, Nano-Micro Lett. 9 (2017) 15, http://dx.doi.org/10.1007/s40820-016-0116-2.
[20] E.J. Yoo, M. Lyu, J. Yun, C.J. Kang, Y.J. Choi, L. Wang, Resistive switching behavior in organic–inorganic hybrid $CH_3NH_3PbI_3-xClx$ perovskite for resistive random access memory devices, Adv. Mater. 27 (2015) 6170–6175, http://dx.doi.org/10.1002/adma.201502889.
[21] R. Waser, M. Aono, Nanoionics-based resistive switching memories, Nat. Mater. 6 (2007) 833–840, http://dx.doi.org/10.1038/nmat2023.
[22] R. Waser, R. Dittmann, C. Staikov, K. Szot, Redox-based resistive switching memories nanoionic mechanisms, prospects, and challenges, Adv. Mater. 21 (2009) 2632–2663, http://dx.doi.org/10.1002/adma.200900375.
[23] E. Lim, R. Ismail, Conduction mechanism of valence change resistive switching memory: a survey, Electronics 4 (2015) 586–613, http://dx.doi.org/10.3390/electronics4030586.
[24] F.C. Chiu, A review on conduction mechanisms in dielectric films, Adv. Mater. Sci. Eng. 2014 (2014) 1–18, http://dx.doi.org/10.1155/2014/578168.
[25] E.G. Gerstner, D.R. McKenzie, Cycling effects in nitrogen doped tetrahedral amorphous carbon non-volatile memory cells, Solid. State Electron. 44 (2000) 1641–1645, http://dx.doi.org/10.1016/S0038-1101(00)00092-7.
[26] F. Zhuge, R.-W. Li, C. He, Z. Liu, X. Zhou, Non-volatile resistive switching in graphene oxide thin films, Phys. Appl. Graphene Exp. 2 (2011) 421–438, http://dx.doi.org/10.5772/15201.
[27] C. Tsai, F. Xiong, E. Pop, M. Shim, M. Science, F. Seitz, C. Engineering, U. States, Resistive random access memory enabled by carbon nanotube, ACS Nano 7 (2013) 5360–5366.
[28] L. Li, D. Wen, Memory behavior of multi-bit resistive switching based on multiwalled carbon nanotubes, Org. Electron. 34 (2016) 12–17, http://dx.doi.org/10.1016/j.orgel.2016.03.041.
[29] O.A. Ageev, Y.F. Blinov, O.I. Il'in, B.G. Konoplev, M.V. Rubashkina, V.A. Smirnov, A.A. Fedotov, Study of the resistive switching of vertically aligned carbon nanotubes by scanning tunneling microscopy, Phys. Solid State 57 (2015) 825–831, http://dx.doi.org/10.1134/S1063783415040034.
[30] C.E. Cava, C. Persson, A.J.G. Zarbin, L.S. Roman, Resistive switching in iron-oxide-filled carbon nanotubes, Nanoscale 6 (2014) 378–384, http://dx.doi.org/10.1039/c3nr04320g.
[31] Y. Chai, Y. Wu, K. Takei, H.Y. Chen, S. Yu, P.C.H. Chan, A. Javey, H.S.P. Wong, Resistive switching of carbon-based RRAM with CNT electrodes for ultra-dense memory, Tech. Dig. Int. Electron Devices Meet. IEDM (2010) 2–5, http://dx.doi.org/10.1109/IEDM.2010.5703328.

[32] O.A. Ageev, Y.F. Blinov, O.I. Il'in, A.S. Kolomiitsev, B.G. Konoplev, M.V. Rubashkina, V.A. Smirnov, A.A. Fedotov, Memristor effect on bundles of vertically aligned carbon nanotubes tested by scanning tunnel microscopy, Tech. Phys. 58 (2013) 1831–1836, http://dx.doi.org/10.1134/S1063784213120025.
[33] Y. Wu, B. Yang, B. Zong, H. Sun, Z. Shen, Y. Feng, Carbon nanowalls and related materials, J. Mater. Chem. 14 (2004) 469, http://dx.doi.org/10.1039/b311682d.
[34] G. Takyo, S. Kono, T. Goto, H. Sasaoka, K. Nishimura, Origin of field emission from a nano-diamond/carbon nanowall electron emitter, Jpn. J. Appl. Phys. 47 (2008) 2241–2243, http://dx.doi.org/10.1143/JJAP.47.2241.
[35] O. Tanaike, N. Kitada, H. Yoshimura, H. Hatori, K. Kojima, M. Tachibana, Lithium insertion behavior of carbon nanowalls by dc plasma CVD and its heat-treatment effect, Solid State Ion. 180 (2009) 381–385, http://dx.doi.org/10.1016/j.ssi.2009.01.012.
[36] T.C. Hung, C.F. Chen, W.T. Whang, Deposition of carbon nanowall flowers on two-dimensional sheet for electrochemical capacitor application, Electrochem. Solid State Lett. 12 (2009) K41–K44, http://dx.doi.org/10.1149/1.3099325.
[37] B. Yang, Y. Wu, B. Zong, Z. Shen, Electrochemical synthesis and characterization of magnetic nanoparticles on carbon nanowall templates, Nano Lett. 2 (2002) 751–754, http://dx.doi.org/10.1021/nl025572r.
[38] H.F. Yen, Y.Y. Horng, M.S. Hu, W.H. Yang, J.R. Wen, A. Ganguly, Y. Tai, K.H. Chen, L.C. Chen, Vertically aligned epitaxial graphene nanowalls with dominated nitrogen doping for superior supercapacitors, Carbon N. Y. 82 (2015) 124–134, http://dx.doi.org/10.1016/j.carbon.2014.10.042.
[39] V.A. Krivchenko, D.M. Itkis, S.A. Evlashin, D.A. Semenenko, E.A. Goodilin, A.T. Rakhimov, A.S. Stepanov, N.V. Suetin, A.A. Pilevsky, P.V. Voronin, Carbon nanowalls decorated with silicon for lithium-ion batteries, Carbon N. Y. 50 (2012) 1438–1442, http://dx.doi.org/10.1016/j.carbon.2011.10.042.
[40] Z. Bo, S. Mao, Z. Jun Han, K. Cen, J. Chen, K. (Ken) Ostrikov, Emerging energy and environmental applications of vertically-oriented graphenes, Chem. Soc. Rev. 2015 (2015) 97–108, http://dx.doi.org/10.1039/C4CS00352G.
[41] C.A. Santini, A. Sebastian, C. Marchiori, V.P. Jonnalagadda, L. Dellmann, W.W. Koelmans, M.D. Rossell, C.P. Rossel, E. Eleftheriou, Oxygenated amorphous carbon for resistive memory applications, Nat. Commun. 6 (2015) 8600, http://dx.doi.org/10.1038/ncomms9600.
[42] F. Cataldo, Simple generation and detection of polyynes in an arc discharge between graphite electrodes submerged in various solvents, Carbon N. Y. 41 (2003) 2671–2674, http://dx.doi.org/10.1016/S0008-6223(03)00345-2.
[43] G. Compagnini, M. Sinatra, P. Russo, G.C. Messina, O. Puglisi, S. Scalese, Deposition of few layer graphene nanowalls at the electrodes during electric field-assisted laser ablation of carbon in water, Carbon N. Y. 50 (2012) 2362–2365, http://dx.doi.org/10.1016/j.carbon.2012.01.038.
[44] F. Cataldo, Synthesis of polyynes in a submerged electric arc in organic solvents, Carbon N. Y. 42 (2004) 129–142, http://dx.doi.org/10.1016/j.carbon.2003.10.016.
[45] K. Vasu, K. Pramoda, K. Moses, A. Govindaraj, C.N.R. Rao, Single-walled nanohorns and other nanocarbons generated by submerged arc discharge between carbon electrodes in liquid argon and other media, Mater. Res. Express 1 (2013) 15001, http://dx.doi.org/10.1088/2053-1591/1/1/015001.
[46] S.K. Shin, S.M. Park, Preparation of polyynes by the laser ablation of graphite in water and organic solvents, Bull. Korean Chem. Soc. 33 (2012) 597–600, http://dx.doi.org/10.1016/j.apsusc.2010.10.074.
[47] G. Khurana, P. Misra, N. Kumar, S. Kooriyattil, J.F. Scott, R.S. Katiyar, Enhanced resistive switching in forming-free graphene oxide films embedded with gold nanoparticles deposited by electrophoresis, Nanotechnology 27 (2016) 15702, http://dx.doi.org/10.1088/0957-4484/27/1/015702.
[48] R.B. Heimann, S.E. Evsyukov, L. Kavan, Carbyne and carbynoid stuctures, Chem. Phys. Lett. 207 (1999) 480–486, http://dx.doi.org/10.1016/0009-2614(93)89033-E.
[49] L. Kavan, Electrochemical carbyne-like materials, Carbon N. Y. 36 (1998) 801–808.
[50] D. Yang, A. Velamakanni, G. Bozoklu, S. Park, M. Stoller, R.D. Piner, S. Stankovich, I. Jung, D.A. Field, C.A. Ventrice, R.S. Ruoff, Chemical analysis of graphene oxide films after heat and chemical treatments by X-ray photoelectron and Micro-Raman spectroscopy, Carbon N. Y. 47 (2009) 145–152, http://dx.doi.org/10.1016/j.carbon.2008.09.045.
[51] V.A. Krivchenko, S.A. Evlashin, K.V. Mironovich, N.I. Verbitskiy, A. Nefedov, C. Wöll, A.Y. Kozmenkova, N.V. Suetin, S.E. Svyakhovskiy, D.V. Vyalikh, A.T. Rakhimov, A.V. Egorov, L.V. Yashina, Carbon nanowalls: the next step for physical manifestation of the black body coating, Sci. Rep. 3 (2013) 3328, http://dx.doi.org/10.1038/srep03328.
[52] S. Kurita, A. Yoshimura, H. Kawamoto, T. Uchida, K. Kojima, M. Tachibana, P. Molina-Morales, H. Nakai, Raman spectra of carbon nanowalls grown by plasma-enhanced chemical vapor deposition, J. Appl. Phys. 97 (2005), http://dx.doi.org/10.1063/1.1900297.
[53] Haomin Wang, Yihong Wu, C.K.S. Choong, Jun Zhang, Kie Leong Teo, Zhenhua Ni, Zexiang Shen, Disorder induced bands in first order Raman spectra of carbon nanowalls, in: 2006 Sixth IEEE Conf. Nanotechnol, IEEE, 2006, pp. 219–222, http://dx.doi.org/10.1109/NANO.2006.247613.
[54] M. Hiramatsu, M. Hori, Carbon Nanowalls, Springer Vienna, Vienna, 2010, http://dx.doi.org/10.1007/978-3-211-99718-5.
[55] G. Khurana, P. Misra, R.S. Katiyar, Forming free resistive switching in graphene oxide thin film for thermally stable nonvolatile memory applications, J. Appl. Phys. 114 (2013) 124508, http://dx.doi.org/10.1063/1.4823734.
[56] I. Musa, D. Munindrasdasa, G. Amaratunga, W. Eccleston, Ultra-low-threshold field emission from conjugated polymers, Nature 395 (1998) 362–365, http://dx.doi.org/10.1038/26444.
[57] Y.J. Fu, F.J. Xia, Y.L. Jia, C.J. Jia, J.Y. Li, X.H. Dai, G.S. Fu, B.Y. Zhu, B.T. Liu, Bipolar resistive switching behavior of La 0.5 Sr 0.5 CoO 3−σ films for nonvolatile memory applications, Appl. Phys. Lett. 104 (2014) 223505, http://dx.doi.org/10.1063/1.4881720.
[58] S. Pei, H.M. Cheng, The reduction of graphene oxide, Carbon N. Y. 50 (2012) 3210–3228, http://dx.doi.org/10.1016/j.carbon.2011.11.010.
[59] K. Yu, Z. Bo, G. Lu, S. Mao, S. Cui, Y. Zhu, X. Chen, R.S. Ruoff, J. Chen, Growth of carbon nanowalls at atmospheric pressure for one-step gas sensor fabrication, Nanoscale Res. Lett. 6 (2011) 202, http://dx.doi.org/10.1186/1556-276X-6-202.